



Published in final edited form as:

Biofabrication. ; 13(3): . doi:10.1088/1758-5090/ac0964.

Green electrospinning for biomaterials and biofabrication

Christopher Z Mosher¹, Philip A P Brudnicki¹, Zhengxiang Gong¹, Hannah R Childs¹, Sang Won Lee¹, Romare M Antrobus¹, Elisa C Fang¹, Theanne N Schiros^{2,3}, Helen H Lu^{1,2,*}

¹Biomaterials and Interface Tissue Engineering Laboratory, Department of Biomedical Engineering, Columbia University, New York, NY 10027, United States of America

²Materials Research Science and Engineering Center, Columbia University, New York, NY 10027, United States of America

³Science and Mathematics Department, Fashion Institute of Technology, New York, NY 10001, United States of America

Abstract

Green manufacturing has emerged across industries, propelled by a growing awareness of the negative environmental and health impacts associated with traditional practices. In the biomaterials industry, electrospinning is a ubiquitous fabrication method for producing nano- to micro-scale fibrous meshes that resemble native tissues, but this process traditionally utilizes solvents that are environmentally hazardous and pose a significant barrier to industrial scale-up and clinical translation. Applying sustainability principles to biomaterial production, we have developed a ‘green electrospinning’ process by systematically testing biologically benign solvents (U.S. Food and Drug Administration Q3C Class 3), and have identified acetic acid as a green solvent that exhibits low ecological impact (global warming potential (GWP) = 1.40 CO₂ eq. kg/L) and supports a stable electrospinning jet under routine fabrication conditions. By tuning electrospinning parameters, such as needle-plate distance and flow rate, we updated the fabrication of widely utilized biomedical polymers (e.g. poly- α -hydroxyesters, collagen), polymer blends, polymer-ceramic composites, and growth factor delivery systems. Resulting ‘green’ fibers and composites are comparable to traditional meshes in terms of composition, chemistry, architecture, mechanical properties, and biocompatibility. Interestingly, material properties of green synthetic

* Author to whom any correspondence should be addressed. hllu@columbia.edu.

Credit authorship contribution statement

Christopher Z Mosher: Conceptualization; Data curation; Formal analysis; Funding acquisition; Investigation; Methodology; Validation; Visualization; Writing—original draft; Writing—review & editing. Philip A P Brudnicki: Conceptualization; Data curation; Formal analysis; Investigation; Methodology; Validation; Writing—review & editing. Zhengxiang Gong: Data curation; Formal analysis; Investigation; Writing—review & editing. Hannah R Childs: Formal analysis; Investigation; Methodology; Validation; Writing—review & editing. Sang Won Lee: Formal analysis; Investigation; Methodology; Validation; Writing—review & editing. Romare M Antrobus: Formal analysis; Investigation; Validation; Writing—review & editing. Elisa C Fang: Formal analysis; Investigation; Validation; Writing—review & editing. Theanne N Schiros: Conceptualization; Data curation; Investigation; Methodology; Resources; Software; Supervision; Validation; Visualization; Writing—review & editing. Helen H Lu: Conceptualization; Data curation; Funding acquisition; Methodology; Project administration; Resources; Software; Supervision; Validation; Writing—original draft; Writing—review & editing.

Supplementary material for this article is available [online](#)

Data availability statement

All data that support the findings of this study are included within the article (and any supplementary files).

Conflict of interest

The authors declare no competing interest.

fibers are more biomimetic than those of traditionally electrospun fibers, doubling in ductility (91.86 ± 35.65 vs. $45 \pm 15.07\%$, $n = 10$, $p < 0.05$) without compromising yield strength (1.32 ± 0.26 vs. 1.38 ± 0.32 MPa) or ultimate tensile strength (2.49 ± 0.55 vs. 2.36 ± 0.45 MPa). Most importantly, green electrospinning proves advantageous for biofabrication, rendering a greater protection of growth factors during fiber formation (72.30 ± 1.94 vs. $62.87 \pm 2.49\%$ alpha helical content, $n = 3$, $p < 0.05$) and recapitulating native ECM mechanics in the fabrication of biopolymer-based meshes ($16.57 \pm 3.92\%$ ductility, 33.38 ± 30.26 MPa elastic modulus, 1.30 ± 0.19 MPa yield strength, and 2.13 ± 0.36 MPa ultimate tensile strength, $n = 10$). The eco-conscious approach demonstrated here represents a paradigm shift in biofabrication, and will accelerate the translation of scalable biomaterials and biomimetic scaffolds for tissue engineering and regenerative medicine.

Keywords

green manufacturing; green electrospinning; biofabrication; tissue engineering; biomaterials; fiber; scaffold

1. Introduction

In the late 20th century, a series of legislation was passed in the United States establishing corporate manufacturing requirements related to emitted air pollution, wastewater management, hazardous waste disposal, and chemical usage. The Toxic Substances Control Act, first implemented in 1976 and continuously amended to-date, limits industrial use of chemical substances that pose an unreasonable risk to human health or to the environment. In response, manufacturing methods have evolved to adhere to such governmental regulation while also considering the Planetary Boundaries Framework, which sets quantifiable limits on global environmental disturbances that are caused by human activity [1–3]. For example, in the textile industry, businesses that adopt green manufacturing and management methods such as a circular supply chain, recycling, and upcycling [4] have a demonstrated competitive advantage with lower production costs, expanded customer bases, improved company image, and innovative fabrication strategies [5]. In contrast, in the biomaterials and medical device industry, recently estimated to total 156 billion globally with 40% located in the United States [6], eco-friendly manufacturing practices remain nascent. Given the pivotal role biomaterials play in healthcare and the treatment of cardiovascular, musculoskeletal, and neurodegenerative disorders [7], there is a significant need as well as opportunity to implement large-scale green manufacturing of biomaterials in the medical device field.

The demand for eco-friendly and translatable scale-up of biomaterial production is underscored by the emergence of biofabrication or ‘building with biology’, pertaining to the use of cells, extracellular matrix (ECM), and/or biomaterials to produce intricate living or non-living biological products [8]. In 2009, one of the largest awards in the history of the National Science Foundation was granted to build a statewide alliance for biofabrication in South Carolina [9]. A natural application of biofabrication is tissue engineering, where biodegradable scaffolds formed via popular fabrication methods such as electrospinning are used to guide cell-mediated regeneration of grafts to replace tissue lost from injury or

disease [10]. Outside of tissue engineering, bio-manufactured products have been broadly applied in drug screening, environmental toxicology studies and more recently, complex *in vitro* models of diseased and healthy tissues [11, 12]. Moreover, biofabrication has already entered the green technology market with biofuels being produced as a sustainable energy source [13], and bio-based food [14] and leather [15, 16] emerging as alternatives to animal-based products that otherwise exemplify poor stewardship. Implementation of green biofabrication processes will undoubtedly accelerate this revolution in biodesign and manufacturing.

After its first demonstration in the 1990s to generate nanoscale fibers [17, 18], electrospinning has become the pre-eminent method for producing nanometer- to micrometer-diameter fibers that can be seeded with cells for tissue engineering or other biofabrication applications [19–21]. This method is unique in its ability to produce meshes with organization and/or architecture comparable to the native ECM, such as a collagen fibril (nm) or fiber (μm). In the past decade, over 500 PubMed-indexed scientific papers describing such electrospun technologies have been published (supplemental figures 1(a) and (b) (available online at stacks.iop.org/BF/13/035049/mmedia)). These functionalized polymeric fibers are designed for a variety of clinical applications, such as biofabrication of biological tissues [22–26], modeling of the ECM [27, 28], or serving as platforms for T-cell therapy [29]. Coupled with a burgeoning industry of manufacturers located across the globe [30], electrospinning has become a mainstay in biofabrication for tissue regeneration.

Traditional electrospinning methods begin with solubilizing a polymer in common industrial solvents such as trifluoroethanol (TFE), dimethylformamide (DMF), or dichloromethane (DCM). The resulting polymer melt is prepared in a syringe fitted with an electrically charged micrometer-diameter needle, and the syringe plunger is advanced at a specified rate. As the applied electric field overcomes the surface tension of extruded droplets, fibers are ejected from the needle onto a collecting plate which grounds the electrical charge [17, 18]. Ultimately, a porous mesh made of fibers with a high surface area to volume ratio is formed [31, 32]. Parameters such as the polymer flow rate, voltage, needle-collecting plate distance, needle gauge, and relative humidity of the surrounding environment have a great impact on fiber diameter and morphology [33, 34]. These may be tuned to produce fibrous matrices composed of several functionalizable polymers including polylactide-*co*-glycolide (PLGA), poly-*ε*-caprolactone (PCL), and collagen (e.g. gelatin) [35]. Furthermore, it has been demonstrated that growth factors such as bone morphogenetic protein 2 (BMP-2) [36, 37], insulin-like growth factor 1 (IGF-1) [38], and transforming growth factor β 3 (TGF- β 3) [39], as well as ceramic nanoparticles including hydroxyapatite [40, 41] and calcium deficient apatite (CDA) [42], can be incorporated into electrospun scaffolds during fiber formation with some maintenance of their bioactivity.

Despite research success, the clinical translation of electrospun technologies is severely hindered by a myriad of challenges in scaling up for biomanufacturing, ranging from the environmental risks of volatile solvent storage and disposal at large volumes, to meeting health and safety standards during both fabrication and implementation [43]. The ecological damage associated with solvents used in the electrospinning process is often overlooked. Moreover, electrospun fibers may contain trace amounts of solvents post-fabrication, and

common solvents used for electrospinning such as TFE, DMF, or DCM are restricted from use in pharmaceuticals by the U.S. Food and Drug Administration (FDA) [44]. To mitigate these risks, we aim to develop a method for green electrospinning, which will facilitate scale-up and clinical translation of electrospun technologies that are safe for manufacturers and patients, while minimizing manufacturing impact on the environment. In the following sections, we describe green electrospinning of biopolymer nanofibers and synthetic polymer microfibers that act as matrices to support cell-based biofabrication. Additionally, we show that green electrospun fibers can be incorporated with ceramic nanoparticles or growth factor in a manner that is similar or, in many aspects, better than traditionally electrospun fibers, with broader applications in tissue engineering and biofabrication. Taken together, these data demonstrate that green electrospinning represents a new paradigm for 21st century biomaterial and scaffold manufacturing.

2. Materials and methods

2.1. Solvent impact analysis

For each solvent of interest (table 1), manufacturing impacts pertaining to ecological damage, human health damage, and resource depletion were determined by life cycle assessment (LCA) methodology using Sustainable Minds[®] Life Cycle Assessment software and the EcoInvent database. All impacts were calculated assuming a functional unit of 1 liter solvent manufactured, with the overall impact weighted across categories and expressed in relative mPts/L for direct comparison where one point (Pt) represents an average individual's annual share of the total environmental impact in the United States. A cradle-to-gate partial product life cycle was performed from resource extraction (cradle) to the factory gate which includes manufacturing of the solvents, with use and disposal omitted; such assessments are often used as the basis for environmental product declarations.

2.2. Fiber fabrication

Micro- and nano-fibers were fabricated by electrospinning with a custom device [17, 20]. Briefly, the synthetic polymers polylactide-*co*-glycolide (PLGA 50:50, DL, $\overline{M}_w \approx 106$ kDa, IV = 0.6/0.8 dL/g, Lakeshore Biomaterials) and poly- ϵ -caprolactone (PCL, $\overline{M}_n \approx 70 - 90$ kDa, PDI < 2, Sigma-Aldrich) were solubilized at a 5:1 weight ratio in a 2:3 mixture of *N,N*-dimethylformamide (DMF, Sigma-Aldrich) to dichloromethane (DCM, Sigma-Aldrich) for traditional electrospinning, or as listed in table 1, FDA Q3C Class 3 solvents such as glacial acetic acid (Sigma-Aldrich) for 'green electrospinning'. The resulting polymer melt (32% w/v) was vortexed (Vortex Genie 2, Scientific Industries) for 1 h. For all solvents tested, a stable electrospin is defined as spinning for at least 1 h without needing to unclog the needle or clear its opening of debris.

For ceramic incorporation, calcium deficient apatite (CDA, Sigma-Aldrich) particles were mixed with the solvent, sonicated (80 W, Ultrasonic Cleaner FS20, Thermo Fisher Scientific) for 1 h, and added to the polymer melts described previously (10, 15, or 20% w/w CDA/polymer). Resulting melts (41% w/v) were vortexed for 2 h and electrospun using the same parameters described for ceramic-free PLGA/PCL fibers (figure 3(a)). To incorporate growth factor within the microfibers, bovine serum albumin (BSA, 5% w/w, Sigma-Aldrich)

was combined with the PLGA/PCL polymer melt described above for 1 h of vortexing, followed by the addition of insulin-like growth factor-1 (IGF-1, 100 μg , 5 ng/mL, Gibco Laboratories) and an additional 1 h of mixing. Traditional and green solutions were electrospun using the parameters listed in figure 4(a). Last, biopolymer nanofibers were fabricated by solubilizing gelatin (porcine-derived, ~300 g bloom, type A, Sigma-Aldrich) in TFE (7% w/v, Sigma-Aldrich) or 50% v/v acetic acid in water (20% w/v gelatin) for traditional and green electrospinning, respectively. Resulting solutions were vortexed for 1 h, and electrospun using the parameters listed in figure 5(a).

2.3. Fiber characterization

Fibrous scaffolds were characterized using discs ($\text{Ø} = 10 \text{ mm}$) measuring $100 \pm 20 \mu\text{m}$ in thickness that were cut from electrospun meshes with a biopsy punch (Sklar Surgical Instruments). Fiber diameter and morphology were evaluated by performing scanning electron microscopy (SEM, 5 kV, Zeiss Sigma VP) on samples that were pre-coated with gold-palladium (4 nm) to reduce charging effects (108 Auto, Cressington Scientific). Fiber diameter was quantified via ImageJ (National Institutes of Health) analysis of resulting SEM micrographs (5000X, $n = 50$ fibers/group) [27]. Energy dispersive x-ray analysis (EDXA, XFlash[®] 6 \times 30 Detector, Esprit 2.1 software, Bruker) was performed for 300 s at 10 kV to obtain quantitative spectra and colorized micrographs for the elements carbon (green), calcium (blue), and phosphorus (red). Additionally, intensity profiles for calcium and phosphorus were measured through individual fibers.

Scaffold contact angle ($n = 5$) in ambient conditions was determined by ellipsometry (Fiber-Lite[®] Model 190, Dolan-Jenner Industries), by placing the sample upon a stage, depositing a 10 μl deionized water droplet the scaffold surface, and immediately measuring the angle between the convex drop profile and the flat scaffold using a fiber optic illuminator fixed to a protractor telescope lens apparatus.

Chemical composition was assessed using Fourier transform infrared spectroscopy in attenuated total reflectance mode (FTIR-ATR, $n = 3$, Spectrum 100, Perkin Elmer). The spectra were collected (100 scans, spectral resolution 4 cm^{-1}) and analyzed for characteristic PLGA [46–48], PCL [49], or gelatin [50–52] peaks.

Crystal structure of as-fabricated scaffolds was analyzed by x-ray diffraction (XRD, $n = 3$, PANalytical XPert3 Powder XRD, Malvern Panalytical). Samples were loaded onto a zero-diffraction plate (silicon, p-type, β -doped, MTI Corporation, Richmond, CA) and scanned through a 1 cm nickel-based beam mask from 20–30 $^\circ(2\theta)$ with a step size of 0.029 $^\circ$ and a beam path utilizing 1/4 $^\circ$ anti-scatter and 1/8 $^\circ$ divergence slits. Resulting x-ray diffractograms were analyzed for semi-crystalline peaks corresponding to the orthorhombic planes present in PCL [53], as well as the crystal planes characteristic of CDA (JCPDS 9–432). Gelatin fibers were evaluated for a broad characteristic peak representing amorphous gelatin [54], with additional crystalline planes identified [55].

The ASTM International standard test method for tensile properties of plastics (D638-14) was used to perform uniaxial tensile testing [20, 56]. Briefly, scaffolds (6 \times 1 cm, $n = 10$) were mounted with custom clamps onto a microtester device (Instron, Model 5848) with an

average gauge length of 3 cm, and evaluated to failure at a strain rate of 5 mm/min. Scaffold yield strength, ultimate tensile stress, and ductility were determined, with elastic modulus calculated as the slope of the linear region of resulting stress–strain curve.

To assess degradation, as-fabricated PLGA/PCL scaffolds were immersed in ITS media at 37 °C and 5% CO₂. The ITS media consists of Dulbecco's Modified Eagle's Medium (DMEM, Thermo Fisher Scientific) supplemented with 1% insulin, transferrin, selenous acid (ITS+) premix (BD Biosciences), 1% penicillin–streptomycin (P/S, 10 000 U/mL penicillin, 10 mg/mL streptomycin), 0.1% gentamicin sulfate, 0.1% antifungal (250 µg/mL amphotericin B), and 40 µg/mL L-proline (Sigma-Aldrich). All antibiotics and antifungals were purchased from Corning Inc. At selected time points (up to 16 weeks), samples were rinsed in distilled water, dried in a CentriVap Concentrator (Labconco Co.) until completely dry, and weighed to evaluate fiber degradation.

The mineral content of as-fabricated scaffolds was assessed with thermogravimetric analysis (TGA, $n = 3$, Q50, TA Instruments). Briefly, samples were loaded into calibrated platinum pans, suspended beneath a thermocouple within a furnace, and heated in nitrogen by 20 °C/min to 100 °C. The temperature was then increased in oxygen to 700 °C, followed by an increase to 900 °C in nitrogen. As PLGA (50:50) and PCL completely degrade at 500 °C [57] and 489 °C [58], respectively, the residual weight corresponded to the weight of mineral remaining in the scaffold. Thus, weight percent mineral content was determined by dividing the ash weight by the original scaffold weight. To evaluate mineral particle size and distribution, machine learning was employed (supplemental figures 3(a)–(d)). Briefly, EDXA images of CDA particles ($n = 15$) were rotated 360° in 10° intervals with mirrored edges, and corresponding label maps were created ($n = 540$). Sematic segmentation of the images and maps was performed, and 70% were used for training ($n = 378$) with 30% used as the test set ($n = 162$). A custom built convolutional neural network consisting of 91 layers was trained, validated with the test set, and used to evaluate EDXA images of CDA-containing fibers ($n = 10$). The output segmentation results quantified the size and spatial distribution of the CDA particles embedded within the fibers.

2.4. Cells and cell culture

Neonatal (1–7 d old) bovine tibiofemoral joints were acquired from a local abattoir (Green Village Packing Co.), and primary articular chondrocytes and synovium-derived stem cells were isolated following published protocols [59, 60]. Prior to harvest, the joints were soaked in detergent for 40 min followed by 70% ethanol for 20 min to sterilize. In an aseptic environment, a #22 scalpel blade (feather, Thermo Fisher Scientific) was used to remove the muscle, subcutaneous fascia, collateral ligaments, patellar tendon, adipose tissue, and medial and lateral menisci covering the cartilage, and the joint capsule was opened. Following, full thickness cartilage was extracted from the femoral groove and condyles, minced with the scalpel blade, and digested for 16 h in digestion medium at 37 °C and 5% CO₂. Digestion medium consisted of 0.1% (w/v) collagenase II (Worthington Biochemical Corporation) in DMEM supplemented with 10% fetal bovine serum (FBS, Atlanta Biologicals), 2% P/S, 0.2% gentamicin sulfate, and 0.2% antifungal. After 16 h, isolated cells were passed through a sterile 30 µm nylon macroporous filter (Spectra/Mesh®, Cole-Palmer Instrument Co.) to

remove ECM components, and resulting full thickness chondrocytes were maintained in high-density culture (4×10^5 cells cm^{-2}) in fully-supplemented DMEM containing 10% FBS, 1% non-essential amino acids, 1% P/S, 0.1% gentamicin sulfate and 0.1% antifungal for 3 d before seeding.

For stem cell isolation, the synovial membrane lining the femoral condyles was harvested and digested for 4 h at 37 °C and 5% CO_2 in digestion medium with similar composition to that above, but with a Minimum Essential Medium Alpha (α MEM, Corning) base. The digested slurry was filtered and centrifuged, and synovium-derived stem cells were cultured (1.8×10^3 cells cm^{-2}) in fully-supplemented α MEM. To eliminate synovium-derived macrophages and obtain a homogeneous stem cell population, cells were subsequently expanded on tissue culture plastic (up to passage 4) [39] prior to seeding onto fibers.

To seed isolated cells onto fibrous scaffolds, 10 μl of concentrated cell suspension was pipetted onto each scaffold to achieve a seeding density of 100 000 cells cm^{-2} and allowed to attach for 25 min at 37 °C and 5% CO_2 . Following, cell-laden scaffolds were submerged in 1.5 mL ITS media (chondrocytes) or fully-supplemented α MEM (stem cells) and cultured at 37 °C and 5% CO_2 , with media refreshed three times weekly.

2.5. Biocompatibility and phenotypic cell response

Cell viability—Cell viability ($n = 2$) on the scaffolds was visualized using Live/Dead staining (Molecular Probes) following the manufacturer's protocol. Stained samples were rinsed in phosphate buffered saline (PBS, Thermo Fisher Scientific) and immediately imaged under confocal microscopy (Olympus Fluoview IX70) at excitation and emission wavelengths of 488 nm and 515 nm, respectively. To evaluate cell proliferation ($n = 5$), a Quanti-iT™ PicoGreen® dsDNA assay kit (Molecular Probes) was used following the manufacturer's suggested protocol on lysed, ultrasonicated, and papain-digested (18 h) cellular scaffolds. Fluorescence was measured with a microplate reader (Tecan SpectraFluor Plus) at excitation and emission wavelengths of 485 nm and 535 nm, respectively. Measured fluorescence intensity was correlated to a DNA standard curve, and a conversion factor of 7.7 pg DNA/cell [61] was used to determine the total cell number in each sample.

Total **collagen and proteoglycan synthesis** were quantified from sample lysates digested to solubilize the matrix proteins. For collagen content ($n = 5$), a hydroxyproline assay [62] was used. Briefly, aliquots of the sample digest were mixed with 2N sodium hydroxide (Sigma-Aldrich) and heated to 250 °C for 25 min in order to hydrolyze the collagen. The hydrolysate was then oxidized at room temperature for 25 min with buffered Chloramine-T reagent (Sigma-Aldrich) prior to the addition of Ehrlich's reagent (15% p-dimethylaminobenzaldehyde in 2:1 isopropanol/perchloric acid, Sigma-Aldrich). Absorbance was measured at 555 nm with a microplate reader (Tecan SpectraFluor Plus) and hydroxyproline content for each sample was determined by correlating measured optical density to a bovine collagen I solution (Biocolor) standard curve. For glycosaminoglycan (GAG) quantification ($n = 5$), a modified 1,9-dimethylmethylene blue (DMMB) dye-binding assay [63, 64] was used. Samples were mixed with the DMMB dye (pH 3.5) and absorbance was immediately measured (μ Quant, Bio-Tek) at both 540 nm and 595 nm, with the difference between these measurements used to improve the signal detection sensitivity.

Proteoglycan content was determined by correlating measured absorbance to a chondroitin-6-sulfate (Sigma-Aldrich) standard curve.

For **matrix distribution**, histology samples ($n = 3/\text{stain}$) were rinsed with PBS and chemically fixed for 24 h at 4 °C in 10% neutral buffered formalin containing 1% cetylpyridinium chloride (Sigma-Aldrich). The samples were again rinsed in PBS, then soaked overnight in 5% (w/v) polyvinyl alcohol (PVA, Sigma-Aldrich) followed by frozen sectioning with a cryotome (7 μm , CM3050 S, Leica Biosystems). Slides were cleared of PVA by soaking in deionized water for 30 min, and the distribution of collagen was visualized by staining in 0.1% picosirius red for 1 h and rinsing in 0.01 M HCl. The proteoglycan matrix was stained with safranin-o for 20 min, Weigert's hematoxylin for 7 min, and fast green counterstain for 12 min. Coverslipped (Cytoseal XYL) samples were imaged under light microscopy (Olympus DP72).

Cell mineralization potential—Cell mineralization potential was assessed by quantifying alkaline phosphatase (ALP) activity ($n = 5$), measured using a colorimetric assay based on the dephosphorylation of p-nitrophenyl phosphate (pNP-PO₄) to p-nitrophenol (pNP) [65]. Prior to sample digestion, an aliquot of the sample lysate was mixed with pNP-PO₄ solution (Sigma-Aldrich) at a 1:1 v/v ratio and incubated at 37 °C for 10 min. Following, absorbance was measured (Tecan SpectraFluor Plus) at 405 nm. The ALP activity of each sample was determined by correlating measured optical density to a pNP standard curve.

2.6. Protein structure and release

The helical structure of a model protein, BSA, was evaluated in simulated electrospinning conditions using circular dichroism spectroscopy. Briefly, ground BSA was solubilized in filtered (0.22 μm , Thermo Fisher Scientific) deionized water or the electrospinning solvents of interest (DMF:DCM or acetic acid) at the same concentration described above for spinning IGF-1-containing fibers (*see* Fiber Fabrication). These solutions were vortexed for 1 h to mimic to the electrospinning protocol, and dried completely via evaporation under airflow. All samples were reconstituted in filtered deionized water (0.1 mg/mL), and 3 scans/sample (0.85 s/point) were obtained from 180 to 250 nm at 25 °C with a 1 nm step size and a 1 nm bandwidth using quartz cells with a 0.5 mm path length (ProData Chirascan V100, Applied Photophysics). The water contribution to each spectrum was subtracted, the spectra were averaged ($n = 3$ per solvent), and data were expressed in terms of mean residue ellipticity (MRE, degree * cm²/dmol), with the α helical content of BSA in each solvent quantified using the 222 nm method [66].

Additionally, IGF-1 was incorporated into electrospun fibers and its release was quantified. Fibrous scaffold discs ($\varnothing = 10$ mm) were cored from an IGF-1-containing mesh (100 μg) using a biopsy punch, and sterilized via exposure to ultraviolet light (15 min/side). The discs were immersed in ITS media (~2.2 mg/mL) and incubated for 3 weeks at 37 °C and 5% CO₂, with media collected and replaced every 3 d such that perfect sink conditions were maintained. Supernatant IGF-1 concentration was quantified via enzyme-linked immunosorbent assay (ELISA, $n = 5$, R&D Systems) according to the manufacturer's

protocol. Briefly, samples were added directly to assay diluent in a prepared plate and incubated for 2 h at 4 °C. Each well was washed four times before incubation for 1 h with IGF-1 conjugate at 4 °C. The conjugate was removed, the wells were washed four times, and substrate solution was added to each well and allowed to react in the dark. Stop solution was added after 30 min, absorbance was measured at 450 nm and 570 nm with a microplate reader (Tecan SpectraFluor Plus), and the difference was used to calculate IGF-1 concentration based on a standard curve.

2.7. Statistical analyses

Results are presented as mean \pm standard deviation, with ' n ' equal to the number of samples analyzed per study group. Multiple trials were conducted to ensure reproducibility and only data from the same representative trials are shown. All data were tested for normality and equal variance between groups. One-way analysis of variance (ANOVA) was performed to determine the effect of solvent type on fiber diameter, tensile mechanical properties, contact angle, scaffold ash weight, ceramic particle size and spatial distribution, BSA α helical content, and IGF-1 incorporation. Two-way ANOVA was used to determine the temporal effects of solvent type on scaffold degradation, (fold-change in) cell number, population doublings, doubling time, ALP activity, GAG and collagen deposition, and IGF-1 release. The Tukey–Kramer post-hoc test was then used for all pair-wise comparisons with significance attained at $p < 0.05$. All statistical analyses were performed using JMP IN statistical software (SAS Institute).

3. Results and discussion

3.1. Green electrospinning: solvent selection criteria

Traditional material synthesis and fabrication practices have resulted in significant environmental and human health consequences, precipitating the design challenge to develop green manufacturing processes within the fields of implantable biomaterials and regenerative medicine. In particular, electrospinning methods for fabricating nano- and micro-scale fibrous scaffolds must be revamped for clinical translation, as traditional solvents prevalent in the literature are highly carcinogenic, elicit extreme eutrophication, and are related to global warming. The first step in implementing green electrospinning is the identification of a non-volatile solvent that is able to solubilize the polymer and enable the formation of a fibrous mesh, maintain bioactivity, support biocompatibility, and facilitate scale-up with minimal negative impacts on health and the environment. Solvent selection is critical here as, while most of the solvent used will evaporate or be removed post-electrospinning, the solvent-polymer interactions during fabrication will affect not only resultant polymer crystallinity and scaffold structure, but also the functionality of incorporated biomolecules and proteins. We began with an extensive review of all published electrospinning studies in the past decade, and found that DMF or its blend with DCM represents the most popular traditional solvent, used in more than half of publications in the last ten years for electrospinning PCL, also the most commonly electrospun polymer. This is followed by TFE, which is routinely used to electrospin collagen (Fig. S1a–b). Interestingly, there is a small number of publications (<10%) exclusively using water, formic acid or acetic acid alone or in combination, which are potential green solvent candidates.

Next, we categorized the known electrospinning solvents and green solvent candidates according to FDA Q3C standards [44]. While adherence to Q3C standards does not constitute FDA approval, these are established FDA recommendations for solvent limits in drugs and biomedical products. This classification system is based on published data describing solvent genotoxicity, carcinogenicity, reproductivity toxicity, and metabolism in mice, rats, and humans, as well as environmental impact when supporting data was available. The solvents are separated into three classes with decreasing toxicity, where Class 1 solvents are inherently toxic and should only be used if they impart significant therapeutic effects. Traditional electrospinning solvents including DMF and DCM are designated Class 2, indicating inherent toxicity with the permitted daily exposure (PDE) limited to 8.8 and 6.0 mg/d, respectively. Consequently, the search for a green solvent candidate was restricted to those in Class 3, as they are designated as biologically benign and non-hazardous for pharmaceutical use by the FDA with allowable PDE of up to 50 mg/d. Moreover, greater exposure to Class 3 solvents is considered acceptable under good manufacturing practice, with acetic acid's PDE established at 3200 mg/d.

Following classification of the solvent candidates (table 1), the ability of each to solubilize common polymers such as PLGA and PCL, as well as to produce a stable electrospin from the polymer blend solution (5:1, 32% w/v), as defined by drawing of a fiber from the syringe and subsequent formation of a 100 μ m thick mesh, was evaluated. Notably, acetic acid was the only Class 3 solvent tested that was capable of sufficient polymer solubilization and subsequent fiber formation. While polymer melts formed in acetone and formic acid, stable electrospins were not possible within routine fabrication parameters [38] used for electrospinning (voltage, needle-plate distance, needle gauge, relative humidity, and flow rate, figure 1(a)). It is likely that with its boiling point and conductivity falling between those of DMF and DCM, the polymer melt formed with acetic acid is likely better suited for electrospinning. Moreover, with sufficient similarities in solvent and polymer chemistry, it is anticipated that acetic acid can readily solubilize the poly(α -hydroxyester) family of polymers (PLA, PGA, PLGA, PCL) as well as other polymers (e.g. polyester, polyethylene, nylon) that are widely utilized as biomaterials or for tissue regeneration.

To evaluate the ecological impacts of solvents, we performed LCA within the EcoInvent database [67]. Ecological damage is comprised of acidification (kg SO₂ eq), ecotoxicity (CTUe), eutrophication (kg N eq), global warming (kg CO₂ eq), and ozone depletion (kg CFC-11 eq). Human health damage includes carcinogenics and non-carcinogenics (both in units of CTUh), respiratory effects (kg PM_{2.5} eq, fine particulates), and smog (kg (ground level) O₃ eq), while resource depletion exclusively refers to diminution of fossil fuels (MJ surplus). It was found that the popular electrospinning solvents (DCM, DMF, TFE) are detrimental to both environmental and human health (figures S2(a) and (b), results expressed in relative mPts of impact per liter of solvent), especially during manufacturing. For instance, given its documented carcinogenicity, the manufacturing of DCM is a significant contributor to human health damage, responsible for the majority of the solvent's 0.32 mPts/L total impact score. In contrast, the much higher total impact score of 0.80 mPts/L for DMF arises predominately from ecological damage attributed to solvent-induced eutrophication of water systems. Eutrophication, in which excess nutrient salts cause algae and cyanobacteria to bloom, leads to the formation of dead zones where the concentration of

dissolved oxygen is too low to support life. Moreover, these dead zones release methane and nitrous oxide into the atmosphere which have about 36- and 300-fold greater GWP than carbon dioxide, respectfully [68]. Furthermore, according to the Planetary Boundary Framework, genetic diversity and the biochemical flows of nitrogen and phosphorus have already exceeded safe operating limits [2, 3] and contributed to documented global climate change [69, 70]. Such consequences are exacerbated by TFE, which exhibits the greatest manufacturing impact score of all solvents assessed (5.18 mPts/L), translating to a GWP of 211.28 CO₂ eq. kg/L. Collectively, the significant carcinogenicity, eutrophication, and global warming impacts of traditional electrospinning solvents renders them impractical for industrial use and biomedical applications. In contrast, non-volatile solvents such as acetic acid are associated with relatively minimal manufacturing impacts (0.12 mPts/L), with a GWP that is two orders of magnitude lower than that of TFE (1.40 CO₂ eq. kg/L). Moreover, acetic acid can be produced from natural gas with no emissions and only power as a byproduct [71], making it much more scalable and environmentally friendly than traditional solvents.

Based on its ability to support stable electrospinning and documented lower health and ecological impacts, acetic acid was selected here as a model green solvent for electrospinning. To test the efficacy and evaluate the broad applicability of green electrospinning, we conducted a series of studies described below aimed at comparing polymeric meshes formed through either traditional (TFE, DMF, and DCM) or green (acetic acid) electrospinning methods. It is anticipated that both structural organization and material properties, as well as biocompatibility of the meshes, will be independent of fabrication method. Additionally, given the detrimental properties of traditional solvents, green electrospinning will be more favorable for biofabrication, especially in terms of forming robust biopolymer fibers and incorporating biofactors.

3.2. Green vs. traditional: synthetic polymer fibers and phenotypic cell response

To test the effects of green manufacturing on synthetic polymer fiber formation, we compared a polymeric blend of PLGA and PCL made using traditional and green electrospinning (figures 1(a)–(e)). This mesh formulation was selected as it comprises of the two most common biodegradable polymers in the field, and has been successfully tested for graft-host integration *in vitro* and *in vivo* [38]. The traditional 2:3 DMF:DCM solvent mixture was used to yield fibers with a diameter measuring $1.21 \pm 0.21 \mu\text{m}$, while green electrospinning with acetic acid resulted in a fiber diameter of $1.28 \pm 0.11 \mu\text{m}$, with no significant difference in either fiber morphology or diameter evident via scanning electron microscopy (SEM, figure 1(a)). Of note, the polymer melt viscosity was greater in green compared to traditional solvents, and thus the flow rate was slowed in order to ensure the spin of a mesh with comparable fiber diameter, although fabrication can also be optimized by increasing the applied voltage. After 24 h of drying under a vacuum to remove any residual solvent, contact angle was also similar between these groups ($n = 5$, $^{\wedge}p < 0.05$), indicating fiber surface energy was unaffected by solvent choice.

Maintenance of chemical structure was also confirmed via ATR (figure 1(c)), where characteristic peaks for carbonyl stretching (C=O) in PCL [49] and PLGA [48] were

observed at 1726 cm^{-1} and 1746 cm^{-1} , respectively, with methyl (C–H, 1452 cm^{-1}), ether (C–O–C, 1080 and 1183 cm^{-1}), and carbon-oxygen (C–O, 1129 cm^{-1}) stretch peaks attributed to the presence of PLGA [46–48] detected in both fiber types. Surprisingly, differences in crystal structure were observed with XRD (figure 1(d)). While both fiber types exhibited two semi-crystalline peaks at $2\theta = 21.4^\circ$ and $2\theta = 23.8^\circ$, corresponding to the orthorhombic planes (110) and (200) in PCL [53], the traditionally electrospun fibers had an extra peak at $2\theta = 24.4^\circ$ attributed to splitting of the (200) plane, not present in the polymer pellet control or the green mesh. This suggests that a change in PCL structure occurred after interaction with traditional solvents, while the crystal structure was preserved in acetic acid.

Electrospinning has been reported to alter polymer chain arrangement, typically increasing crystallinity and associated mechanical properties of the fibers compared to pre-processed polymer pellets [72]. The draw ratio, or the ratio of fiber velocity at the collection plate to the velocity of the polymer solution ejected from the syringe, can be used to estimate molecular orientation. The greater draw ratio required for traditional electrospinning likely aligned polymer chains along the fiber axis and lead to the formation of crystallites. This is supported by the larger area under crystalline peaks in traditional fiber XRD compared to green fibers, as well as the slightly slower degradation in traditional vs. green fibers (0.675 ± 0.002 vs. $0.721 \pm 0.010\%$ mass/day, respectively, $n = 5$, $^*p < 0.05$, figure 1(b)). These data suggest the crystal structure difference between groups affected hydrolytic degradation rate. Interestingly, the lack of biologically relevant ductility that has long plagued synthetic polymers is mitigated by green electrospinning, which resulted in a 47% increase in ductility accompanied by a 29% reduction in elastic modulus, without compromising either yield strength or ultimate tensile strength ($n = 10$, $^*p < 0.05$, figure 1(e)). Mechanical behavior of the green mesh is thus more representative of the collagen-rich ECM in connective tissues such as the skin [73, 74], with an elastic modulus of 32 MPa reported for a human type I collagen fibril [75] and a ductility ranging from 42% to 62% reported for human skin [76].

To assess biocompatibility, we compared cell response on traditional and green meshes *in vitro* (figures 2(a)–(d)). While viable on both types of meshes, articular chondrocytes proliferated faster with more population doublings when cultured on the green mesh ($n = 5$, $^*p < 0.05$ over time, $^*p < 0.05$ between groups), resulting in a significantly greater cell number by day 7 (figure 2(a)). In terms of matrix production, GAG (figure 2(b)) and collagen (figure 2(c)) deposition similarly increased over time on both fiber types ($n = 5$, $^*p < 0.05$), with no differences seen between groups. Histology revealed early matrix deposition on the surface of the scaffolds, with GAG and collagen penetrating throughout the scaffold depths by day 21 in both fiber types. The ALP activity did not differ between groups (figure 2(d)), further confirming maintenance of the articular chondrocyte phenotype. Collectively, these data demonstrate that green electrospinning yields comparable microfiber meshes that support cell attachment, growth, and phenotypic expression. Notably, green electrospinning better preserves polymer crystal structure and produces a more ductile mesh that mimics native ECM mechanics. Additionally, the green mesh is biocompatible and promotes cell growth, and offers significant functional advantages over traditional approaches.

3.3. Green vs. traditional: composite polymer fibers

Expanding on the applicability of green electrospinning and inspired by the composite nature of biological tissues, we next compared polymer-ceramic fiber fabrication using green and traditional methods (figures 3(a)–(d)). The ceramic selected was CDA, a mineral source with a semi-crystalline, calcium-deficient structure reminiscent of carbonated hydroxyapatite (HA) found in native bone [77, 78]. Addition of calcium phosphate has been reported to enhance chondrocyte proliferation, matrix deposition, and mineralization potential in hydrogels [42], indicating it is an optimal ceramic source for stimulating calcification. Applying this strategy to fibrous scaffolds, traditional (DMF/DCM) and green (acetic acid) electrospinning were used to fabricate PLGA/PCL fibers containing 20% (w/w) CDA, with comparable average fiber diameters of 0.97 ± 0.45 and $0.92 \pm 0.19 \mu\text{m}$, respectively (figure 3(a), SEM, $n = 50$ fibers/group). Ceramic nanoparticles were well-distributed within the fibers, and EDXA intensity profiles confirmed Ca and P presence along the fiber (blue = Ca, red = P, figure 3(a)). Ceramic incorporation was found to fibers, be within 1% (w/w) of target values (19.92 ± 0.44 and $20.14 \pm 0.62\%$ for traditional and green respectively, figure 3(b)). In terms of crystal structure, semi-crystalline peaks corresponding to the (110) and (200) planes inherent in PCL [53], along with the crystal planes (002, 211, 300, and 202) characteristic of CDA [42] (JCPDS 9–432) were identified with both meshes (figure 3(c)). The fidelity of nanoparticle incorporation and distribution (EDXA images, $n = 1500+$ particles) were evaluated using a convolution neural network customized for image segmentation (Fig. S3a–d), as nanoparticle aggregation often leads to inhomogeneities in composite meshes. The machine learning algorithm revealed that the fibers were doped with predominantly particles with an area between 0 and $0.1 \mu\text{m}^2$ and the particles were consistently spaced along the fiber length (figure 3(d)), with no difference in particle size or spatial distribution found between electrospinning methods. When seeded with stem cells derived from the knee synovium [39], the green meshes supported cell growth over time, with significantly higher cell growth when compared to a ceramic-free control (figure S4). Collectively, these results demonstrate that similar to the traditional method, green electrospinning can be readily used to generate biocompatible polymer-ceramic composite fibers with uniform particle size and distribution, without altering mesh fiber diameter or architecture.

3.4. Expediting biofabrication: incorporation and release of growth factor

Exercising temporal distribution of key growth factors is essential for high fidelity and expedited biomanufacturing, and one of the present challenges in this field is to preserve the bioactivity of biomolecules during scaffold fabrication. We compare here the incorporation and release of the model growth factor IGF-1 (7.6 kDa) from green and traditional fibers (figures 4(a) and (b)), as IGF-1 delivery from an electrospun mesh has been shown to enhance chondrocyte migration, proliferation and differentiation [39]. Moreover, insulin-like proteins, receptors, ligands, and proteases collectively referred to as the ‘IGF axis’ are known to regulate several tissues, including cartilage, bone, and neurons. Bovine serum albumin (BSA) has been shown in prior studies to protect bioactivity of growth factors in a dose-dependent manner [38, 39, 79, 80], and given that it is similar in protein structure with IGF-1, circular dichroism (CD) analysis was performed (figure 4(c)) to identify conformational changes when immersed in traditional (DMF/DCM) or green solvents

(acetic acid, deionized water). It was observed that the α helical content of BSA, as derived from mean residue ellipticity, is significantly greater in acetic acid ($72.30 \pm 1.94\%$) and water ($78.90 \pm 4.95\%$) as compared to DMF/DCM ($62.87 \pm 2.49\%$, $n = 3$, $^{\wedge}p < 0.05$), with no difference measured between water and acetic acid. These findings confirm the protective effects of green solvents, with loss of protein structure only evident in the spectra when exposed to volatile chemicals such as DMF and DCM. While interactions with BSA (66.5 kDa) shield IGF-1 (7.6 kDa) from degradation during electrospinning, it is likely that green solvents further preserve secondary structure to allow the factor to remain bioactive once released.

Electrospinning was then optimized for fabricating traditional and green meshes pre-loaded with IGF-1 (figure 4(a)), again yielding meshes with uniform and comparable fiber diameter (1.28 ± 0.24 vs. $1.27 \pm 0.23 \mu\text{m}$, respectively, $n = 50/\text{group}$). No significant difference in contact angle ($n = 5$) was observed between groups, suggesting that the surface energy of the fibers was similar. Interestingly, an ELISA revealed that significantly more IGF-1 was incorporated in green meshes ($n = 5$, $^{\wedge}p < 0.05$) and most importantly, the factor remained bioactive, further confirming the protective effects of green solvents (figure 4(b)). In terms of release kinetics, significantly more IGF-1 was released from green meshes at 24 h ($n = 5$, $^{\wedge}p < 0.05$), likely due to the faster degradation of the green fibers. By day 4, no significant difference in cumulative IGF-1 release between groups was evident with the total amount of IGF-1 released comparable between groups by day 22. It is clear that green solvents are not detrimental to protein structure and, in fact, result in greater yield of bioactive factor post-fabrication, making their use more advantageous for growth factor-based biofabrication strategies.

3.5. Biomimetic manufacturing: production of ECM-like meshes

Collagen is the most abundant protein in the body, accounting for ~90% of ECM composition. Interactions between cells and the collagenous matrix give rise to signaling cues that regulate cell behavior including growth and differentiation, and are essential for tissue homeostasis and repair [81]. Unsurprisingly, collagen is also one of the first materials to be explored as a scaffold for tissue engineering, albeit with little success due to limitations in recapitulating its continuous and interwoven fibrous structure; often, the same structure and composition that give biopolymers like collagen unique properties also makes them very difficult to process into ECM analogs. Consequently, despite its biomimetic potential, the use of collagen has been restricted to self-assembled weak hydrogels (1–10 kPa), as well as glutaraldehyde crosslinked gels that form sheets with relatively inferior mechanical properties and low structural stability in the body. Thus, a persistent challenge in biofabrication is the production of biomimetic and functional ECM-like meshes based on collagenous fibers.

Harnessing the potential to preserve native ECM composition, gelatin, which is composed of soluble protein peptides that are isolated from hydrolyzed collagen, is one of the most commonly engineered biopolymers with broad applications in cell and drug delivery, as well as skin, bone, cartilage, and cardiovascular tissue engineering [82]. Testing the potential of green electrospinning for biopolymer mesh production, gelatin nanofibers were electrospun

in either TFE or in acetic acid, and the chemical, structural, and mechanical properties were compared between these two methods (figures 5(a)–(d)). Electrospinning parameters such as polymer weight percent (7 vs. 20% w/v) and flow rate (2.5 vs. 1.0 mL/h) were optimized to ensure no significant difference in fiber diameter between methods, with 149 ± 17 nm and 149 ± 22 nm measured for traditional and green fibers, respectively ($n = 50$ fibers/group, figure 5(a)). No structural difference between mesh type were detected (ATR, $n = 3$, figure 5(b)), with characteristic amide bands A (3306 cm^{-1}), B (3076 cm^{-1}), I (1646 cm^{-1}), II (1520 cm^{-1}), and III (1234 cm^{-1}) attributed to gelatin [50–52, 83–85] present in both. In terms of crystal structure ($n = 3$, figure 5(c)), all fibers evaluated by XRD displayed a broad peak at $2\theta = 21.8^\circ$, signifying the presence of amorphous gelatin as reported in literature [54] and confirmed by XRD of pure gelatin powder. In both traditional and green gelatin nanofiber diffractograms, additional peaks corresponding to the crystal planes (002), (111), (310), and (222) [55] are present, suggesting the material becomes more atomically organized after electrospinning due to changes in polymer chain arrangement.

Not surprisingly, these changes in crystal structural are reflected in the tensile mechanical properties of the electrospun mesh, with much higher mechanical properties evident than those reported for self-assembled collagen gels [86, 87]. Interestingly, significant differences in material properties were found between the green and traditional groups (figure 5(d)). While the Young's modulus remained unchanged (33.83 ± 2.87 vs. 30.26 ± 4.51 MPa), the ultimate tensile strength (2.13 ± 0.36 vs. 0.67 ± 0.03 MPa), yield strength (1.30 ± 0.19 vs. 0.62 ± 0.04 MPa), and ductility (16.57 ± 3.92 vs. $5.58 \pm 1.18\%$) significantly improved with green electrospinning ($n = 10$, $p < 0.05$). This unique structure-function augmentation may be attributed to carboxymethylation and subsequent covalent crosslinking of the biopolymers by acetic acid, which has been shown to enhance elastic and viscous moduli previously [88]. Specifically, the trifunctional intermolecular cross-link histidinohydroxylysinonorleucine has been reported as a marker of collagen maturation, especially in skin [89]. In this context, the increased ductility achieved with green electrospinning is clinically advantageous, approximating those of commercially available human dermis allografts pre- (AlloPatch[®]) and post-processing (GRAFTJACKET[™]) which each fail around 60% elongation [90]. Taken together, these results show that green gelatin fibers recapitulated traditional nanofiber diameter, chemistry, and crystal structure, albeit with significantly improve tensile mechanical properties. Clearly, green electrospinning can be used to manufacture biopolymer nanofibers that better mimic the native collagenous ECM in structure and function, with the ability to achieve relevant mechanical properties for tissue engineering applications.

To our knowledge, this study is the first direct comparison of green and traditional electrospinning methods spanning multiple polymer systems and solvents, wherein FDA guidelines and LCA are considered collectively and systematically to support industrial scale-up and clinical translation. In the literature, the term 'green electrospinning' has been used to refer to electrospinning water-soluble polymers including chitosan and poly(vinyl alcohol) in order to eliminate dangerous organic solvents from the process [91–96], and has been expanded here to describe electrospinning with other non-volatile solvents including acetic acid and formic acid. While formic acid has been reported for electrospinning of silk [97] and PCL fibers [49, 98], it did not yield blends of PLGA and PCL under standard

electrospinning conditions in this study, suggesting that further optimization is needed and this will be investigated in future studies. In contrast, acetic acid proved particularly facile in its ability to solubilize and readily electrospin PLGA/PCL blends, composite fibers, and fibers based on biopolymers. Moreover, green electrospinning preserved growth factor bioactivity and imparted physiologically relevant mechanical properties to collagen fibers, improving both elastic and viscoelastic properties.

4. Conclusions

Green electrospinning is shown to have broad applicability while being uniquely suited for biofabrication, resolving several key challenges that are unattainable with current approaches: from enhancing biomolecule preservation and preservation of raw material properties, to the fabrication of ECM analogs with biomimetic mechanical properties. Moreover, non-volatile biologically benign solvents (FDA Q3C Class 3) such as acetic acid are superior for industrial scale-up with lower manufacturing impact, resulting in more than an order of magnitude reduction in ecotoxicity, eutrophication, global warming and ozone depletion impacts when compared to traditional solvents utilized in the field. The transformation of electrospinning from a process with detrimental environmental and health impacts to the scalable, eco-conscious ‘green’ electrospinning demonstrated here is both significant and timely, and will engender a paradigm shift in biomaterial fabrication and related practices.

Supplementary Material

Refer to Web version on PubMed Central for supplementary material.

Acknowledgments

This work was supported by the National Institutes of Health (NIH-NIAMS 1R01-AR07352901A), the New York State Stem Cell ESSC Board (NYSTEM C029551), the DoD CDMRP award (W81XWH-15-1-0685), and the National Science Foundation Graduate Research Fellowship (DGE-1644869, CZM). The CD analysis system was supported by NIH grant 1S10OD025102-01, and T N S was supported as part of the NSF MRSEC program through Columbia in the Center for Precision Assembly of Superstratic and Superatomic Solids (DMR-1420634). The authors thank Wing Ki Chan and Eva Hansen for their contributions to the development of the ceramic particle electrospinning method, and Jenny Wang for her help with preparing published electrospinning paper tables.

References

- [1]. Rockström J et al. 2009 A safe operating space for humanity Nature 461 472–5 [PubMed: 19779433]
- [2]. Steffen W. et al. 2015; Planetary boundaries: guiding human development on a changing planet. Science. 347 :1259855. [PubMed: 25592418]
- [3]. Sala S, Benini L, Crenna E and Secchi M 2016 Global environmental impacts and planetary boundaries in LCA JRC Technical Report (European Commission)
- [4]. Beamon BM 1999 Designing the green supply chain Logist. Inf. Manage 12 332–42
- [5]. Rusinko C 2007 Green manufacturing: an evaluation of environmentally sustainable manufacturing practices and their impact on competitive outcomes IEEE Trans. Eng. Manage 54 445–54
- [6]. US Department of Commerce and International Trade. The medical technology industry in the United States. Medical Technology Spotlight; 2020.

- [7]. Xue J, Wu T, Dai Y and Xia Y 2019 Electrospinning and electrospun nanofibers: methods, materials, and applications *Chem. Rev* 119 5298–415 [PubMed: 30916938]
- [8]. Mironov V, Trusk T, Kasyanov V, Little S, Swaja R and Markwald R 2009 Biofabrication: a 21st century manufacturing paradigm *Biofabrication* 1 022001 [PubMed: 20811099]
- [9]. Nagarkatti P, Kresovich S, Odom J, Markwald R, Dooley RL, Little T and Curtis C 2009 research infrastructure improvement grant (Claflin, Clemson, MUSC, SC State University, and USC) National Science Foundation EPSCoR Research Infrastructure
- [10]. Langer R and Vacanti J 1993 *Tissue engineering Science* 260 920–6 [PubMed: 8493529]
- [11]. Lanza R, Langer R, Vacanti JP and Atala A 2020 *Principles of Tissue Engineering* (New York: Academic)
- [12]. Wobma H and Vunjak-Novakovic G 2016 *Tissue engineering and regenerative medicine 2015: a year in review Tissue Eng. B* 22 101–13
- [13]. Kiefer D, Merkel M, Lilge L, Henkel M and Hausmann R 2021 From acetate to bio-based products: underexploited potential for industrial biotechnology *Trends Biotechnol.* 39 397–411 [PubMed: 33036784]
- [14]. Bhat ZF, Kumar S and Fayaz H 2015 *In vitro* meat production: challenges and benefits over conventional meat production *J. Integr. Agric* 14 241–8
- [15]. Kim D, Kim Y, Kim K and Shin H 2017 Research trend and product development potential of fungal mycelium-based composite materials *Korean Soc. Biotechnol. Bioeng. J* 32 174–8
- [16]. Hildebrandt J, Thrän D and Bezama A 2021 The circularity of potential bio-textile production routes: comparing life cycle impacts of bio-based materials used within the manufacturing of selected leather substitutes *J. Clean. Prod* 287 125470
- [17]. Reneker DH and Chun I 1996 Nanometre diameter fibres of polymer, produced by electrospinning *Nanotechnology* 7 216
- [18]. Doshi J and Reneker DH 1995 Electrospinning process and applications of electrospun fibers *J. Electrostat* 35 151–60
- [19]. Demir MM, Yilgor I, Yilgor E and Erman B 2002 Electrospinning of polyurethane fibers *Polymer* 43 3303–9
- [20]. Moffat KL, Kwei AS-P, Spalazzi JP, Doty SB, Levine WN and Lu HH 2009 Novel nanofiber-based scaffold for rotator cuff repair and augmentation *Tissue Eng. A* 15 115–26
- [21]. Erisken C, Zhang X, Moffat KL, Levine WN and Lu HH 2013 Scaffold fiber diameter regulates human tendon fibroblast growth and differentiation *Tissue Eng. A* 19 519–28
- [22]. Laurencin CT, El-amin SF, Ibim SE, Willoughby DA, Attawia M, Allcock HR and Ambrosio AA 1996 A highly porous 3-dimensional polyphosphazene polymer matrix for skeletal tissue regeneration *J. Biomed. Mater. Res* 30 133–8 [PubMed: 9019476]
- [23]. James R, Kumbar SG, Laurencin CT, Balian G and Chhabra AB 2011 Tendon tissue engineering: adipose-derived stem cell and GDF-5 mediated regeneration using electrospun matrix systems *Biomed. Mater* 6 025011 [PubMed: 21436509]
- [24]. Pham QP, Sharma U and Mikos AG 2006 Electrospinning of polymeric nanofibers for Tissue Engineering applications: a review *Tissue Eng.* 12 1197–211 [PubMed: 16771634]
- [25]. Subramony SD, Dargis BR, Castillo M, Azeloglu EU, Tracey MS, Su A and Lu HH 2013 The guidance of stem cell differentiation by substrate alignment and mechanical stimulation *Biomaterials* 34 1942–53 [PubMed: 23245926]
- [26]. Qu D, Moshier CZ, Boushell MK and Lu HH 2015 Engineering complex orthopaedic tissues via strategic biomimicry *Ann. Biomed. Eng* 43 697–717 [PubMed: 25465616]
- [27]. Lee NM, Erisken C, Iskratsch T, Sheetz M, Levine WN and Lu HH 2017 Polymer fiber-based models of connective tissue repair and healing *Biomaterials* 112 303–12 [PubMed: 27770633]
- [28]. Baker BM and Mauck RL 2007 The effect of nanofiber alignment on the maturation of engineered meniscus constructs *Biomaterials* 28 1967–77 [PubMed: 17250888]
- [29]. Dang AP, de Leo S, Bogdanowicz DR, Yuan DJ, Fernandes SM, Brown JR, Lu HH and Kam LC 2018 Enhanced activation and expansion of T cells using mechanically soft elastomer fibers *Adv. Biosyst* 2 1700167 [PubMed: 31008184]

- [30]. Lagaron J, Solouk A, Castro S and Echegoyen Y 2017 *Electrospun Materials for Tissue Engineering and Biomedical Applications* (Amsterdam: Elsevier) pp 57–72
- [31]. Li W-J, Laurencin CT, Caterson EJ, Tuan RS and Ko FK 2002 Electrospun nanofibrous structure: a novel scaffold for tissue engineering *J. Biomed. Mater. Res* 60 613–21 [PubMed: 11948520]
- [32]. Baker BM, Nerurkar NL, Burdick JA, Elliott DM and Mauck RL 2009 Fabrication and modeling of dynamic multipolymer nanofibrous scaffolds *J. Biomech. Eng* 131 101012 [PubMed: 19831482]
- [33]. Nezarati RM, Eifert MB and Cosgriff-Hernandez E 2013 Effects of humidity and solution viscosity on electrospun fiber morphology *Tissue Eng. C* 19 810–9
- [34]. Pillay V, Dott C, Choonara YE, Tyagi C, Tomar L, Kumar P, Du Toit LC and Ndesendo VMK 2013 A review of the effect of processing variables on the fabrication of electrospun nanofibers for drug delivery applications *J. Nanomater* 2013 789289
- [35]. Xie J, Li X and Xia Y 2008 Putting electrospun nanofibers to work for biomedical research *Macromol. Rapid Commun* 29 1775–92 [PubMed: 20011452]
- [36]. Li C, Vepari C, Jin H-J, Kim HJ and Kaplan DL 2006 Electrospun silk-BMP-2 scaffolds for bone tissue engineering *Biomaterials* 27 3115–24 [PubMed: 16458961]
- [37]. Nie H, Soh BW, Fu Y-C and Wang C-H 2008 Three-dimensional fibrous PLGA/HAp composite scaffold for BMP-2 delivery *Biotechnol. Bioeng* 99 223–34 [PubMed: 17570710]
- [38]. Boushell MK, Moshier CZ, Suri GK, Doty SB, Strauss EJ, Hunziker EB and Lu HH 2019 Polymeric mesh and insulin-like growth factor 1 delivery enhance cell homing and graft–cartilage integration *Ann. New York Acad. Sci* 1442 138–52 [PubMed: 30985969]
- [39]. Qu D, Zhu JP, Childs HR and Lu HH 2019 Nanofiber-based transforming growth factor- β 3 release induces fibrochondrogenic differentiation of stem cells *Acta Biomater.* 93 111–22 [PubMed: 30862549]
- [40]. Khanarian NT, Boushell MK, Guo XE, Doty SB, Strauss EJ, Hunziker EB and Lu HH 2013 Design of a hydrogel-nanofiber scaffold for osteochondral interface tissue engineering *Trans. 59th Annual Meeting of the Orthopaedic Research Society*
- [41]. Boushell MK, Hung CT, Hunziker EB, Strauss EJ and Lu HH 2017 Current strategies for integrative cartilage repair *Connect. Tissue Res* 58 393–406 [PubMed: 27599801]
- [42]. Boushell MK, Khanarian NT, LeGeros RZ and Lu HH 2017 Effect of ceramic calcium–phosphorus ratio on chondrocyte-mediated biosynthesis and mineralization *J. Biomed. Mater. Res. A* 105 2694–702 [PubMed: 28547848]
- [43]. Persano L, Camposeo A, Tekmen C and Pisignano D 2013 Industrial upscaling of electrospinning and applications of polymer nanofibers: a review *Macromol. Mater. Eng* 298 504–20
- [44]. International Council for Harmonisation 2018 *Impurities: guideline for residual solvents Q3C (R7)* p 25
- [45]. Smallwood I *Handbook of organic solvent properties*. Butterworth-Heinemann; 12 2 2012
- [46]. Lu HH, Tang A, Oh SC, Spalazzi JP and Dionisio K 2005 Compositional effects on the formation of a calcium phosphate layer and the response of osteoblast-like cells on polymer-bioactive glass composites *Biomaterials* 26 6323–34 [PubMed: 15919111]
- [47]. Sutton D, Durand R, Shuai X and Gao J 2006 Poly(D,L-lactide-co-glycolide)/poly(ethylenimine) blend matrix system for pH sensitive drug delivery *J. Appl. Polym. Sci* 100 89–96
- [48]. Jose MV, Thomas V, Johnson KT, Dean DR and Nyairo E 2009 Aligned PLGA/HA nanofibrous nanocomposite scaffolds for bone tissue engineering *Acta Biomater.* 5 305–15 [PubMed: 18778977]
- [49]. Liverani L and Boccaccini AR 2016 Versatile production of poly(epsilon-caprolactone) fibers by electrospinning using benign solvents *Nanomaterials* 6 75
- [50]. Xu M, Wei L, Xiao Y, Bi H, Yang H and Du Y 2017 Molecular structural properties of extracted gelatin from Yak skin as analysed based on molecular weight *Int. J. Food Prop* 20 S543–55
- [51]. Thi PPN and Nguyen DH 2016 Gelatin as an ecofriendly natural polymer for preparing colloidal silver@gold nanobranches *Green Process. Synth* 5 467–72
- [52]. Nagai T. 2010; Characterization of acid-soluble collagen from skins of surf smelt (*hypomesus pretiosus japonicus brevoort*). *Food Sci. Nutr.* 1 :59.

- [53]. Chen C-C, Chueh J-Y, Tseng H, Huang H-M and Lee S-Y 2003 Preparation and characterization of biodegradable PLA polymeric blends *Biomaterials* 24 1167–73 [PubMed: 12527257]
- [54]. Xu J, Yan J, Gu Q, Li J and Wang H 2011 Preparation of fluoride-containing gelatin nanofiber scaffold *Mater. Lett* 65 2404–6
- [55]. Wang F, Guo E, Song E, Zhao P and Liu J 2010 Structure and properties of bone-like-nanohydroxyapatite/gelatin/polyvinyl alcohol composites *Adv. Biosci. Biotechnol* 1 185–9
- [56]. Lu HH, Cooper JA Jr., Manuel S, Freeman JW, Attawia MA, Ko FK and Laurencin CT 2005 Anterior cruciate ligament regeneration using braided biodegradable scaffolds: *in vitro* optimization studies *Biomaterials* 26 4805–16 [PubMed: 15763260]
- [57]. Silva MF, Hechenleitner AAW, Irache JM, Aparecido de Oliveira AJAD and Gómez Pineda EAG 2015 Study of thermal degradation of PLGA, PLGA nanospheres and PLGA/maghemite superparamagnetic nanospheres *Mater. Res* 18 1400–6
- [58]. Mohamed A, Finkenstadt VL, Gordon SH, Biresaw G, Palmquist DE and Rayas-Duarte P 2008 Thermal properties of PCL/gluten bioblends characterized by TGA, DSC, SEM, and infrared-PAS *J. Appl. Polym. Sci* 110 3256–66
- [59]. Jiang J, Leong NL, Mung JC, Hidaka C and Lu HH 2008 Interaction between zonal populations of articular chondrocytes suppresses chondrocyte mineralization and this process is mediated by PTHrP *Osteoarthr. Cartil* 16 70–82
- [60]. Sampat SR, O'Connell GD, Fong JV, Egge-aguaron E, Ateshian GA and Hung CT 2011 Growth factor priming of synovium-derived stem cells for cartilage tissue engineering *Tissue Eng. A* 17 2259–65
- [61]. Kim Y-J, Sah RLY, Doong J-YH and Grodzinsky AJ 1988 Fluorometric assay of DNA in cartilage explants using Hoechst 33258 *Anal. Biochem* 174 168–76 [PubMed: 2464289]
- [62]. Reddy GK and Enwemeka CS 1996 A simplified method for the analysis of hydroxyproline in biological tissues *Clin. Biochem* 29 225–9 [PubMed: 8740508]
- [63]. Farndale RW, Sayers CA and Barrett AJ 1982 A direct spectrophotometric microassay for sulfated glycosaminoglycans in cartilage cultures *Connect. Tissue Res* 9 247–8 [PubMed: 6215207]
- [64]. Enobakhare BO, Bader DL and Lee DA 1996 Quantification of sulfated glycosaminoglycans in chondrocyte/alginate cultures, by use of 1,9-dimethylmethylene blue *Anal. Biochem* 243 189–91 [PubMed: 8954546]
- [65]. Lu HH, Kofron MD, El-amin SF, Attawia MA and Laurencin CT 2003 *In vitro* bone formation using muscle-derived cells: a new paradigm for bone tissue engineering using polymer–bone morphogenetic protein matrices *Biochem. Biophys. Res. Commun* 305 882–9 [PubMed: 12767913]
- [66]. Chen Y-H, Yang JT and Chau KH 1974 Determination of the helix and β form of proteins in aqueous solution by circular dichroism *Biochemistry* 13 3350–9 [PubMed: 4366945]
- [67]. Wernet G, Bauer C, Steubing B, Reinhard J, Moreno-Ruiz E and Weidema B 2016 The ecoinvent database version 3 (part I): overview and methodology *Int. J. Life Cycle Assess* 21 1218–30
- [68]. United States Environmental Protection Agency 2020 Understanding Global Warming Potentials (<https://www.epa.gov/ghgemissions/understanding-global-warmingpotentials>) (6 2021)
- [69]. Isbell F et al. 2015 Biodiversity increases the resistance of ecosystem productivity to climate extremes *Nature* 526 574–7 [PubMed: 26466564]
- [70]. Côté IM and Darling ES 2010 Rethinking ecosystem resilience in the face of climate change *PLoS Biol.* 8 e1000438 [PubMed: 20668536]
- [71]. Somiari I and Manousiouthakis V 2018 Coproduction of acetic acid and hydrogen/power from natural gas with zero carbon dioxide emissions *AIChE J.* 64 860–76
- [72]. Baji A, Mai Y-W, Wong S-C, Abtahi M and Chen P 2010 Electrospinning of polymer nanofibers: effects on oriented morphology, structures and tensile properties *Compos. Sci. Technol* 70 703–18
- [73]. Manschot J and Brakkee A 1986 The measurement and modelling of the mechanical properties of human skin *in vivo*—I. The measurement *J. Biomech* 19 511–5 [PubMed: 3745223]
- [74]. Pawlaczyk M, Lelonkiewicz M and Wieczorowski M 2013 Age-dependent biomechanical properties of the skin *Adv. Dermatol. Allergol* 5 302–6

- [75]. Graham JS, Vomund AN, Phillips CL and Grandbois M 2004 Structural changes in human type I collagen fibrils investigated by force spectroscopy *Exp. Cell Res* 299 335–42 [PubMed: 15350533]
- [76]. Haut RC 2002 *Accidental Injury* (Berlin: Springer) pp 228–53
- [77]. LeGeros RZ 2008 Calcium phosphate-based osteoinductive materials *Chem. Rev* 108 4742–53 [PubMed: 19006399]
- [78]. Vallet-Regi M 2004 Calcium phosphates as substitution of bone tissues *Prog. Solid State Chem* 32 1–31
- [79]. Chew SY, Wen J, Yim EKF and Leong KW 2005 Sustained release of proteins from electrospun biodegradable fibers *Biomacromolecules* 6 2017–24 [PubMed: 16004440]
- [80]. Zhu G, Mallery SR and Schwendeman SP 2000 Stabilization of proteins encapsulated in injectable poly (lactide-co-glycolide) *Nat. Biotechnol* 18 52–7 [PubMed: 10625391]
- [81]. Hynes RO and Naba A 2012 Overview of the matrisome—an inventory of extracellular matrix constituents and functions *Cold Spring Harb. Perspect. Biol* 4 a004903 [PubMed: 21937732]
- [82]. van Vlierberghe S, Dubrue P and Schacht E 2011 Biopolymer-based hydrogels as scaffolds for tissue engineering applications: a review *Biomacromolecules* 12 1387–408 [PubMed: 21388145]
- [83]. Di Foggia M, Taddei P, Torreggiani A, Dettin M and Tinti A 2011 Self-assembling peptides for biomedical applications: IR and Raman spectroscopies for the study of secondary structure *Proteomics Res. J* 2 231
- [84]. Muyonga JH, Cole CGB and Duodu KG 2004 Fourier transform infrared (FTIR) spectroscopic study of acid soluble collagen and gelatin from skins and bones of young and adult Nile perch (*Lates niloticus*) *Food Chem.* 86 325–32
- [85]. Cebi N, Durak MZ, Toker OS, Sagdic O and Arici M 2016 An evaluation of Fourier transforms infrared spectroscopy method for the classification and discrimination of bovine, porcine and fish gelatins *Food Chem.* 190 1109–15 [PubMed: 26213083]
- [86]. Yang Y-L, Leone LM and Kaufman LJ 2009 Elastic moduli of collagen gels can be predicted from two-dimensional confocal microscopy *Biophys. J* 97 2051–60 [PubMed: 19804737]
- [87]. Yang Y-L and Kaufman LJ 2009 Rheology and confocal reflectance microscopy as probes of mechanical properties and structure during collagen and collagen/hyaluronan self-assembly *Biophys. J* 96 1566–85 [PubMed: 19217873]
- [88]. Gomez-guillen M and Montero P 2001 Extraction of gelatin from megrim (*Lepidorhombus bosci*) skins with several organic acids *J. Food Sci* 66 213–6
- [89]. Yamauchi M, Woodley DT and Mechanic GL 1988 Aging and cross-linking of skin collagen *Biochem. Biophys. Res. Commun* 152 898–903 [PubMed: 3130057]
- [90]. Barber FA and Aziz-Jacobo J 2009 Biomechanical testing of commercially available soft-tissue augmentation materials *Arthroscopy* 25 1233–9 [PubMed: 19896044]
- [91]. Sun J, Bubel K, Chen F, Kissel T, Agarwal S and Greiner A 2010 Nanofibers by green electrospinning of aqueous suspensions of biodegradable block copolyesters for applications in medicine, pharmacy and agriculture *Macromol. Rapid Commun* 31 2077–83 [PubMed: 21567634]
- [92]. Agarwal S and Greiner A 2011 On the way to clean and safe electrospinning-green electrospinning: emulsion and suspension electrospinning *Polym. Adv. Technol* 22 372–8
- [93]. Krishnan R, Sundarajan S and Ramakrishna S 2013 Green processing of nanofibers for regenerative medicine *Macromol. Mater. Eng* 298 1034–58
- [94]. Liverani L, Vester L and Boccaccini AR 2017 *Electrospun Biomaterials and Related Technologies* (Berlin: Springer) pp 149–68
- [95]. Jiang S, Hou H, Agarwal S and Greiner A 2016 Polyimide nanofibers by “green” electrospinning via aqueous solution for filtration applications *ACS Sustain. Chem. Eng* 4 4797–804
- [96]. Lv D, Zhu M, Jiang Z, Jiang S, Zhang Q, Xiong R and Huang C 2018 Green electrospun nanofibers and their application in air filtration *Macromol. Mater. Eng* 303 1800336
- [97]. Min B-M, Lee G, Kim SH, Nam YS, Lee TS and Park WH 2004 Electrospinning of silk fibroin nanofibers and its effect on the adhesion and spreading of normal human keratinocytes and fibroblasts *in vitro Biomaterials* 25 1289–97 [PubMed: 14643603]

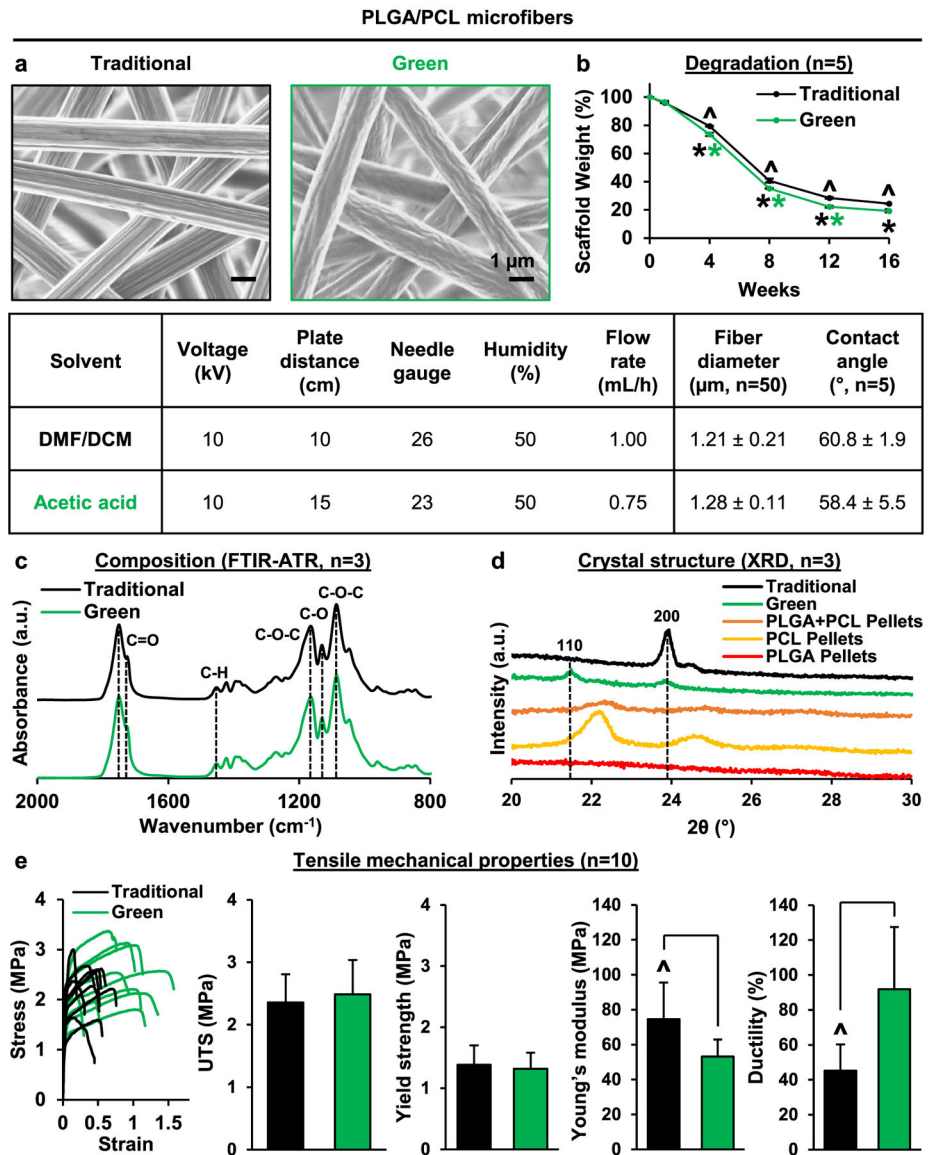
- [98]. Liverani L, Lacina J, Roether JA, Boccardi E, Killian MS, Schmuki P, Schubert DW and Boccaccini AR 2018 Incorporation of bioactive glass nanoparticles in electrospun PCL/chitosan fibers by using benign solvents *Bioact. Mater* 3 55–63 [PubMed: 29744442]

Author Manuscript

Author Manuscript

Author Manuscript

Author Manuscript

**Figure 1.**

Green vs. traditional: electrospinning synthetic polymer fibers. Electrospinning with either acetic acid or traditional solvents (2:3 DMF:DCM) is compared in the fabrication of a polymer-blend mesh [5:1 polylactide-*co*-glycolide (PLGA, 50:50):poly- ϵ -caprolactone (PCL)]. (a) Similar fiber morphology and diameter are observed between methods ($n = 50$ fibers/group). (b) Green fibers measure a greater mass loss per day than traditional fibers (0.721 ± 0.010 vs. $0.675 \pm 0.002\%/day$, $n = 5$, $^{\wedge}p < 0.05$). (c) The representative PLGA and PCL chemical groups (C=O, 1746 and 1726 cm^{-1} ; C-H, 1452 cm^{-1} ; C-O-C, 1183 and 1080 cm^{-1} ; C-O, 1129 cm^{-1}) are present in both green and traditional fibers via Fourier transform infrared spectroscopy in attenuated total reflectance mode (FTIR-ATR, $n = 3$). (d) Crystal structure of PCL is preserved only in green solvents, as indicated by the maintenance of its orthorhombic planes (110, 21.4°; 200, 23.8°) in x-ray diffraction (XRD, $n = 3$), with no peaks evident for PLGA given its amorphous nature. (e) Mechanical properties of green

and traditional fibers were comparable in terms of ultimate tensile strength (UTS) and yield strength, while elastic modulus decreased (29%) and ductility increased (47%) significantly in green fibers ($n = 10$, $^{\wedge}p < 0.05$), better resembling a collagen matrix compared to a traditional mesh.

Author Manuscript

Author Manuscript

Author Manuscript

Author Manuscript

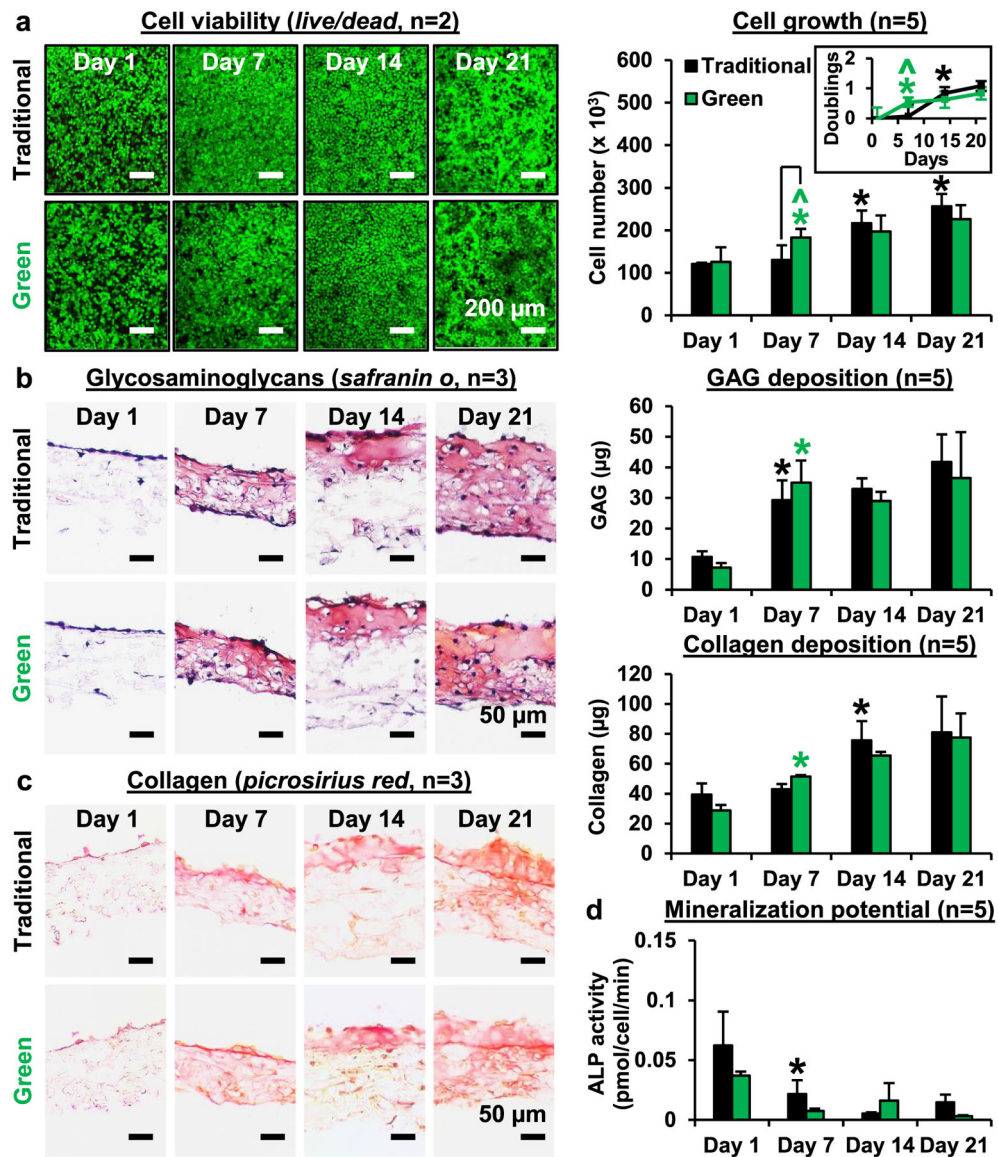


Figure 2. Green vs. traditional: biocompatibility and cell response. Both the green and traditional PLGA/PCL blend fibers are biocompatible, and support comparable cell proliferation and matrix production by articular chondrocytes over three weeks of culture. (a) Significantly greater cell number and population doublings are measured in the green group by day 7 ($n = 5$, $^{\wedge}p < 0.05$ between groups), increasing for both groups over time ($n = 5$, $^*p < 0.05$ over time). (b) Glycosaminoglycan (GAG) and (c) collagen matrix deposition also increase over time ($n = 5$, $^*p < 0.05$), with no significant differences between groups ($^{\wedge}p < 0.05$) evident at any time point. These findings are corroborated by Safranin O and Picosirius Red histological staining ($n = 3$ each) for GAGs and collagen, respectively, which show early surface matrix deposition and penetration of the matrix throughout the scaffold depths by week 1 and over time. (d) No ectopic mineralization is detected on green or tradition mesh (ALP activity, $n = 5$), suggesting chondrocyte phenotype is maintained.

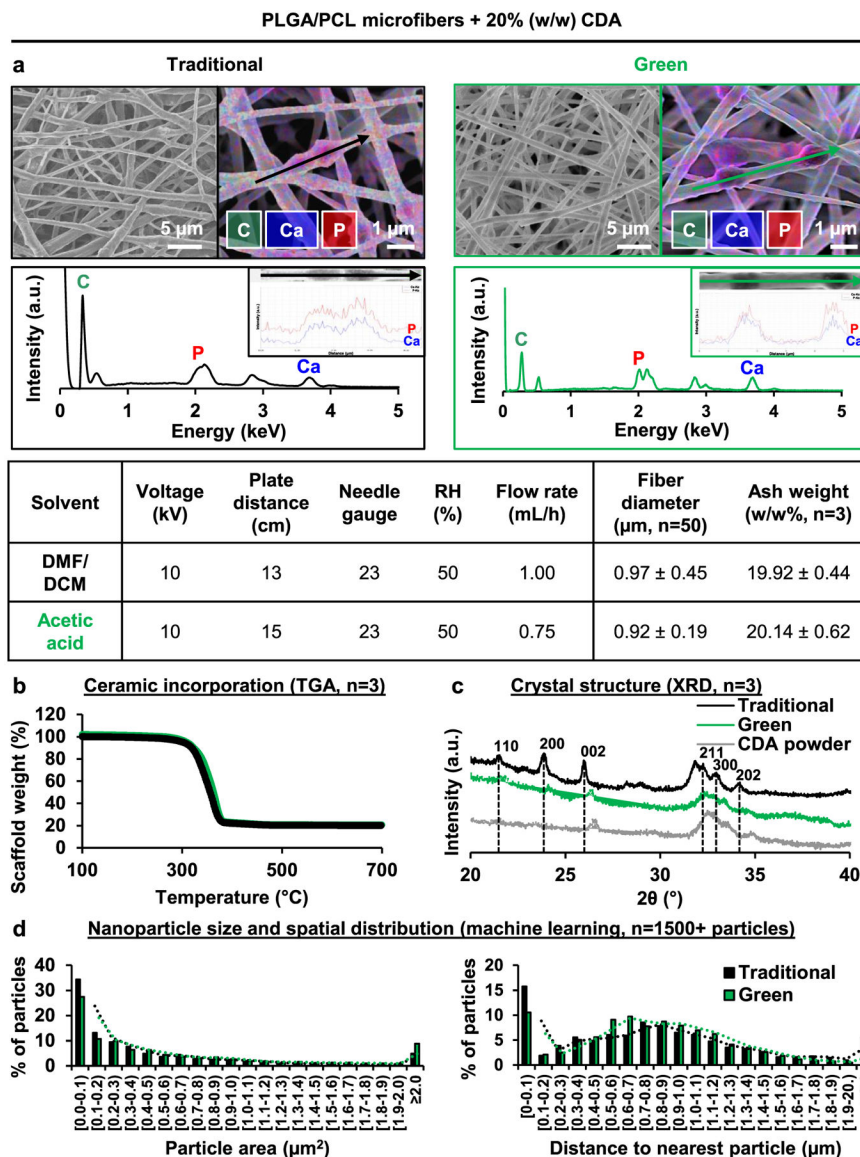


Figure 3. Green vs. traditional: polymer-ceramic composite fibers. Given the biological significance and wide applicability of composite biomaterials, the formation of biomimetic polymer-ceramic composite fibers is compared with green and traditional electrospinning, incorporating calcium-deficient apatite (CDA) into the PLGA/PCL blend fibers. (a) Under optimized electrospinning conditions (RH = relative humidity), the resultant fiber morphology and diameter are similar between groups ($n = 50$ fibers/group). Elemental composition of the fibers determined via energy dispersive x-ray analysis (EDXA, $n = 10$) is also similar, with line profiles along the long fiber axes exhibiting high Ca and P peaks corresponding to CDA particle aggregates. (b) Total ceramic content (20% w/w) is confirmed by thermogravimetric analysis (TGA, $n = 3$). (c) The characteristic crystal planes for PCL (110, 21.4 $^\circ$; 200, 23.8 $^\circ$) and CDA (002, 26.0 $^\circ$; 211, 32.3 $^\circ$; 300, 33.0 $^\circ$; 202, 34.2 $^\circ$) are detectable in x-ray diffraction (XRD, $n = 3$). (d) To quantify incorporated ceramic size

and distribution, a machine learning algorithm utilizing a multi-layer convolutional neural network (CNN) is built to generate histograms of individual CDA nanoparticle area and nearest distance to the nearest particle ($n = 1500+$ particles). No difference is found between fabrication methods.

Author Manuscript

Author Manuscript

Author Manuscript

Author Manuscript

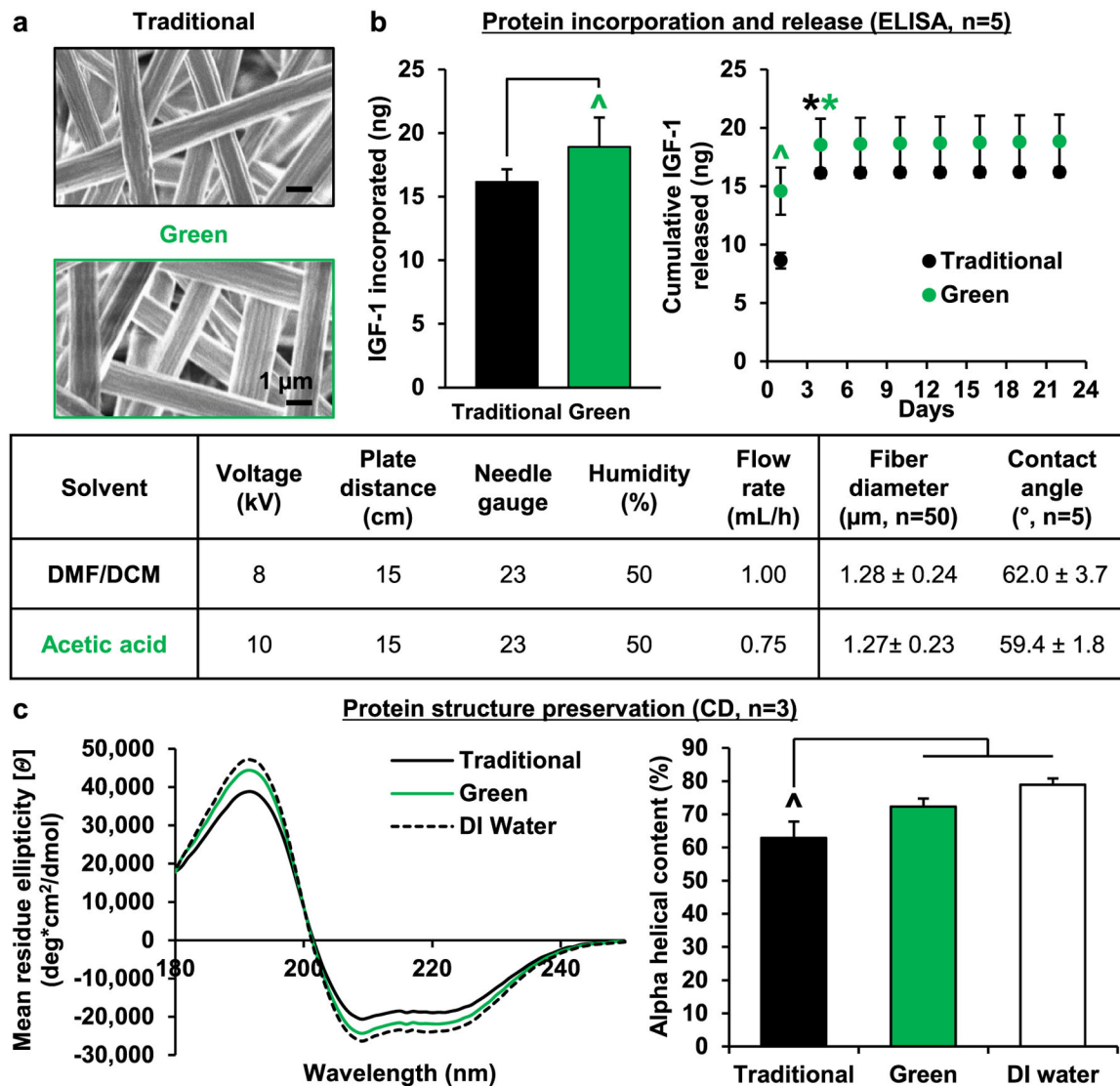
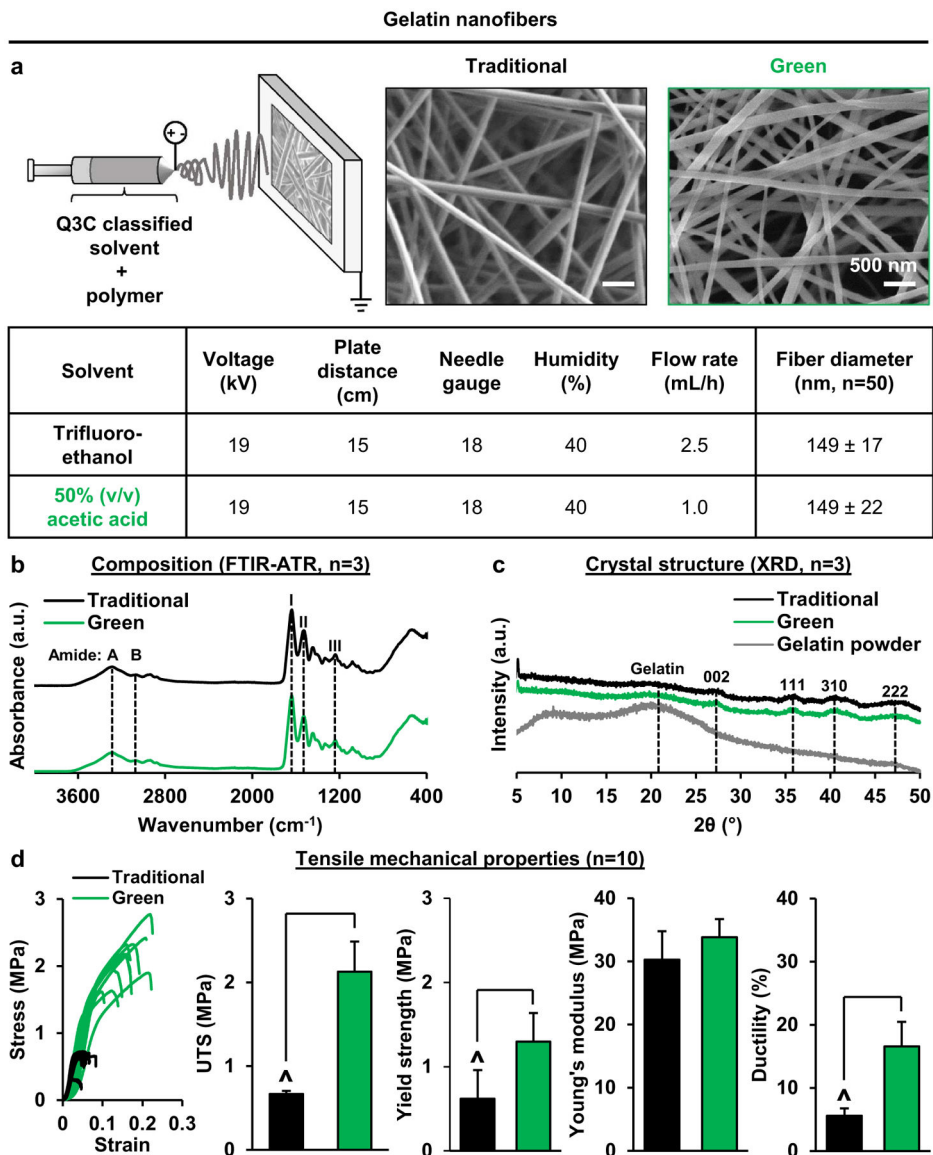
PLGA/PCL microfibers +100 μ g IGF-1 (+40 mg BSA)

Figure 4.

Biofabrication: incorporation of growth factor. To demonstrate further applicability for biofabrication, the incorporation and release of growth factors such as insulin-like growth factor 1 (IGF-1) is evaluated in green vs. traditional electrospinning. (a) No significant difference in fiber morphology, diameter ($n = 50$ fibers/group) or surface energy ($n = 5$) is seen between methods. (b) Significantly greater IGF-1 incorporation is found with green electrospinning ($n = 5$, $^{\wedge}p < 0.05$). After an initially higher IGF-1 burst release, a comparable amount of the factor release was measured over 3 weeks ($n = 5$, $^{\wedge}p < 0.05$ between groups, $^*p < 0.05$ over time). (c) Circular dichroism (CD) analysis reveals that the secondary structure of BSA, which protects IGF-1 during the electrospinning process, is better preserved with green electrospinning. Compared to acetic acid or deionized water, harsh solvents such as DMF/DCM deteriorate the α helical content of BSA (222 nm, $n = 3$, $^{\wedge}p < 0.05$).

**Figure 5.**

Biofabrication: electrospinning of biopolymer. Green electrospinning is applied to the fabrication of biopolymers abundant in the body, using collagen as a model protein. Compared to those formed by traditional methods (7% w/v gelatin in TFE), the green fibers (20% w/v gelatin in 50% v/v acetic acid) are comparable in (a) morphology and size ($n = 50$ fibers/group), as well as (b) composition (FTIR-ATR, $n = 3$) and (c) crystallinity (XRD, $n = 3$). Characteristic chemical groups for gelatin (Amides A, 3306 cm^{-1} ; B, 3076 cm^{-1} ; I, 1646 cm^{-1} ; II, 1520 cm^{-1} ; III, 1234 cm^{-1}) are present in the FTIR-ATR spectra of both green and traditional fibers. An amorphous gelatin peak ($2\theta = 21.8^\circ$) is visible in all XRD diffractograms, with additional planes identified (002, 27.4° ; 111, 35.6° ; 310, 40.3° ; 222, 47.2°) representing an increase in crystallinity after electrospinning with both methods. (d) Green fibers measure a significantly greater UTS, yield strength, and ductility than traditional fibers, with the Young's modulus remaining unchanged ($n = 10$, $^{\wedge}p < 0.05$). The

enhancement may be attributed to covalent crosslinking of collagen by acetic acid during fabrication, with the resulting mesh better approximating the functional properties of a collagenous ECM.

Author Manuscript

Author Manuscript

Author Manuscript

Author Manuscript

Table 1.

Green electrospinning: solvent selection. To demonstrate the feasibility of green electrospinning, FDA regulated Class 3 solvents are compared with traditional electrospinning solvents (TFE, DMF, and DCM), focusing on polymer solubility, stable fiber formation, and manufacturing impact index (Sustainable Minds® Life Cycle Assessment). Acetic acid is the only Class 3 solvent tested with an impact index that measures a fraction of those of traditional solvents, while also solubilizing common synthetic biomedical polymers including PLGA and PCL, and supporting fiber formation under routine electrospinning conditions (5:1 PLGA:PCL, 32% w/v blend, 5–20 kV, 10–15 cm needle-plate distance, 18/23/26G needle gauge, 30%–80% relative humidity, and 0.2–2.5 ml h⁻¹ flow rate).

FDA class	Solvent	Solvent properties				Fabrication objectives			
		Manufacturing impacts (mPts l ⁻¹ h ^a)	Conductivity ($\mu\text{S cm}^{-1}$)	Boiling point (°C)	Solubilizes PLGA	Solubilizes PCL	Forms fiber		
Prohibited	Trifluoroethanol (TFE)	5.18	7.02 ^b	77	✓	✓	✓		
Class 2	Dimethylformamide (DMF)	0.80	0.06	153	✓	✓	✓		
	Dichloromethane (DCM)	0.32	4.30 × 10 ⁻⁵	40					
Class 3	Acetic acid	0.12	0.001	118	✓	✓	✓		
	Acetone	0.09	0.005	56	✓	✓	×		
	Dimethyl sulfoxide	0.13	0.002	189	✓	×	×		
	Ethanol	0.08	0.001	78	×	×	×		
	Formic acid	0.14	5.90 × 10 ⁶	101	✓	✓	×		
	Isopropyl alcohol	0.15	0.06	83	×	×	×		

^aSee supplemental figure 2 for solvent impact index calculations.

^bIndicates measurement with a conductivity probe in ambient conditions, whereas all other conductivity values were obtained from the *Handbook of Organic Solvent Properties* (Smallwood [45]).